Polymers & Polymer Composites, Vol. 25, No. 6, 2017

Author Accepted Manuscript (AAM)

Experimental studies of stiffness degradation and dissipated energy in glass fibre reinforced polymer composite under fatigue loading

M. Ospina Cadavid[1], O. Al-Khudairi[1], H. Hadavinia[1*], D. Goodwin[2], G.H. Liaghat[1]

[1]School of Mechanical & Aerospace Engineering, Kingston University London, SW15 3DW, UK
[2]Offshore Renewable Energy Catapult (ORE), Blyth, Northumberland, NE24 1LZ, UK

Abstract

In this work tensile and compressive properties and fatigue performances of laminated glass fibre reinforced polymer (GFRP) composite under constant amplitude sinusoidal waveform load control at frequency of 5 Hz and at room temperature were investigated for three different types of loading: tension-tension at R= 0.1 and 0.5, reverse loading tension-compression at R= -1 and compression-compression at R= 2 and 10 in fibre and normal to fibre directions. From these series of tests, the corresponding S-N diagrams are obtained. The dynamic stiffness during fatigue loading has shown classical degradation of the GFRP laminates. It is observed that the dynamic modulus decreases with time and the hysteresis loop area changes with some distortion according to the loading condition. Finally hysteresis loops throughout fatigue testing were examined and the variation of energy dissipated per cycle throughout the specimen lifetime was quantified. It is demonstrated that the dissipated energy during the fatigue lifetime is dependent on R-ratio and fibre orientation. However, in majority of the cases, the energy dissipated per cycle near the end of the fatigue lifetime increases as a result of an increase in the area captured by hysteresis loops.

Keywords: Laminated composite; Polymer composite fatigue; S-N diagram; Energy dissipation; Stiffness degradation

* Corresponding author: Dr H Hadavinia T: +44 208417 4864; E: h.hadavinia@kingston.ac.uk

1. Introduction

Laminated fibre reinforced polymer (FRP) composites are the material of choice for advanced engineering structures subjected to continuous fatigue loading such as wind turbine blades when the weight of the structure is a major design constraint. In horizontal axis wind turbine (HAWT), the power train components are subjected to a highly irregular loading condition from turbulent wind flow. The number of fatigue cycles experienced by the blades for 20-30 years design life is of orders of magnitude greater than other rotating machineries. As a result a critical issue regarding applications of GFRP composites in wind turbine and other engineering structures subjected to high cyclic loading is the knowledge about their fatigue reliability under different loading conditions and in different environments.

In FRP composite materials the fracture mechanism is controlled by various combinations of damage modes; including matrix cracking, ply failure, fibre breakage, inter-ply (delamination) and intra-ply (fibre and matrix interface debonding) failure and their respective interactions. Under cyclic loading, the formation of matrix cracks is the beginning of a complex process of interrelated damage events. These may include sequential initiation and accumulation of multiple cracks in all off-axis plies, local interfacial delamination and fibre breakage, which ultimately determine the stiffness degradation, residual strength and lifetime of a given laminate [1, 2].

Delamination is a serious detriment to the stiffness and compressive load carrying capability of a FRP composite laminate [3, 4] and this area has been investigated for new advanced nanomaterial to enhance the fracture toughness of FRP materials [5]. Manjunatha et al. [6] studied the stress-controlled constant amplitude tensile fatigue tests at stress ratio R=0.1 on rubber modified GFRP composites. They showed the fatigue lifetime of GFRP composites laminate increased by a factor of about three times due to the addition of rubber particles in the epoxy matrix.

Quantities related to damage in laminated FRPs, such as fibre-matrix debonding, crack length and density, modulus and residual strength vary during fatigue loading [7]. Also when FRP composites are subjected to spectrum loading or stepped loading, an important and

critical effect called 'load sequence effect' influences the fatigue lifetime and strength degradation of composite materials [8].

For developing predictive models of the strength and lifetime of composite laminates, it is required damage evolution processes thoroughly investigated. The residual stiffness degradation of FRP composite subjected to fatigue loading at various R-ratio need to be quantified and the appropriate parameters should be identified from a series of tensile and fatigue tests and for prediction of the residual stiffness for the laminates [9]. The past studies have shown that the fatigue behaviour of composites is highly dependent on the stress ratio R and the frequency of applied cyclic loading [10, 11, 12, 6, 13].

The present study aims to examine the fatigue performances of laminated glass fibre reinforced polymer (GFRP) composite under constant amplitude sinusoidal waveform load control at frequency of 5 Hz and at room temperature for three different types of loading: tension-tension (T-T) at R= 0.1 and 0.5, reverse loading tension-compression (T-C) at R= -1 and compression-compression (C-C) at R= 2 and 10 in fibre and normal to fibre directions. From these tests the S-N diagrams for various R ratios are obtained. The degradations in dynamic stiffness during fatigue loading of the GFRP laminates are monitored and the causes of the degradation are explored. Finally hysteresis loops throughout fatigue testing are examined to quantify the variation of energy dissipated per cycle throughout the specimen lifetime.

2. Stress-lifetime studies

The S-N tests results are used in many phenomenological models to estimate the fatigue lifetime. The effect of various R ratios on the loading pattern is shown in Fig. 1.

Fatigue test results were analysed by plotting S-N fatigue data on a conventional linear-logarithmic graph. The commonly used models for representing the S-N curve are exponential and power law fatigue models (Basquin 1910) [14]:

$$\sigma = C - D\ log(N_f) \quad (1)$$

$$\sigma = m\ N_f^n \quad (2)$$

In the above equations the stress can be either maximum cyclic stress, or stress amplitude or stress range and N_f is the number of cycles to failure. *C*, *D*, *m* and *n* are constants that can be found from fitting the equations to the experimental fatigue data. The least-squares method was used following the ASTM E 739 standard to obtain parameters m and n [15].

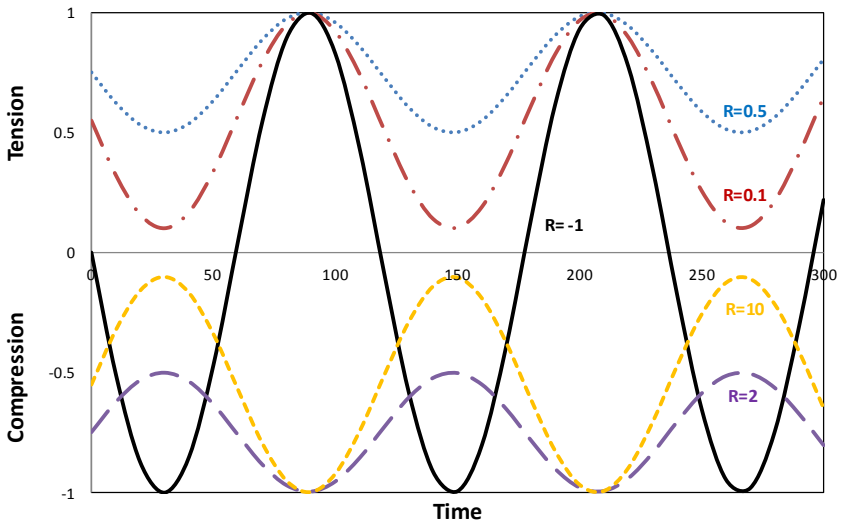

Fig. 1. Constant amplitude load waveforms showing different R-values.

The data obtained from the fatigue tests are used to produce S-N diagrams at different stress ratios for 0° and 90° fibre orientations and exponential law fatigue model coefficient are established. A test frequency of 5 Hz was chosen for this reason.

2.1. Specimen preparation

The dimensions of T-T specimens for all R ratios tested in this study are presented in Fig. 2(a) and they made from 8 layers. Tension-compression and compression-compression specimens could buckle in the compression part of the loading cycle and the height of the specimen should be lower than the critical buckling length to reduce a risk of buckling; as a result the height of gauge length for short specimens was limited to 26 mm while the number of plies increased to 14 layers. The dimensions for T-C and C-C specimens are shown in Fig. 2(b).

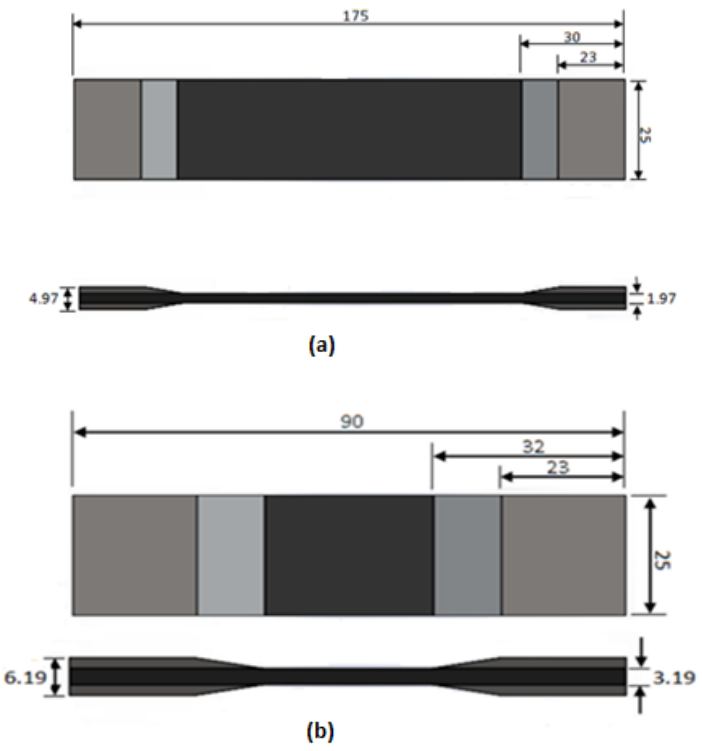

Fig. 2. Fatigue specimen dimensions for (a) tension-tension tests and (b) tension-compression and compression-compression tests.

All GFRP specimens in this work are manufactured by hand lay-up method using a vacuum bag technique using prepreg E-glass fibre/E722 epoxy matrix material supplied by TenCate Ltd. The lay-up of T-T coupon specimens are $[0]_8$ and $[90]_8$, and for T-C and C-C specimens are $[0]_{14}$ and $[90]_{14}$. After curing the specimen, 30mm×25mm×1.5mm aluminium end tabs were bonded to the coupons with ESP110 epoxy adhesive and cured for 60 min at 120^{o}C in order to protect the gripped portions. The edges were then polished, reducing surface flaws.

2.2. Static and fatigue tests

The mechanical properties of the GFRP composite were obtained by performing tensile and compression tests on 0° and 90° fibre orientations according to the standards. The ASTM D 3518-76 standard which recommends the uniaxial tensile stress-strain response of a ±45° laminate which is symmetrically laminated about the midplane is followed for measuring shear strength and shear modulus. The mechanical tests results are summarised in Table 1. The tests were carried out on a MTS universal testing machine with a load cell of 100 kN. The strains are measured by strain gauges bonded in the middle of specimens.

Table 1. Mechanical properties of GFRP laminate measured from experiments.

Material property	
Longitudinal Young's modulus E_{11} (GPa)	36±1
Transverse Young's modulus E_{22} (GPa)	13.0±0.3
Shear Modulus G_{12} (GPa)	4.3±0.6
Poisson's ratio v_{12}	0.220
Tensile strength in fibre direction Xt (MPa)	626±20
Tensile strength normal to fibre direction Yt (MPa)	75±4
Compressive strength in fibre direction Xc (MPa)	230±15
Compressive strength normal to fibre direction Yc (MPa)	180±10
Shear strength S (MPa)	48.7±0.5
Volume fraction	61±2

The fatigue tests on all specimens were carried out under constant amplitude sinusoidal load control using a Zwick/Roell-Amsler HC 25kN servo hydraulic testing machine at a frequency of 5 Hz and force ramp time of 10 second. Different load ratios of T-T at R=0.1, 0.5, T-C at R=-1 and C-C at R=2, 10 were examined. At each stress ratio under examination, 16 specimens were manufactured and tests were carried out at maximum stress between 40-80% of UTS or UCS depending on the R ratio. The laminates stiffness and hysteresis ellipse shaped loop were extracted from corresponding information that was recorded by the machine software at a rate of 40 samples per cycle in a text file.

3. Results of stress lifetime experiments

3.1. The results of S-N tests

The maximum number of cyclic loading was set at 2×10^6 cycles and if the coupon specimen did not fail over this limit, it was terminated prior to fracture. Those specimens which did not fail are marked as run out specimen and showed by an arrow on S-N diagrams. It should be mentioned that the past experimental results shows that conventional polymeric composites do not typically have a fatigue limit, but instead damage progresses during the entire lifetime of the material which causes failure even at very low applied stresses [16].

The results of the S-N diagrams for specimens under T-T loading at R= 0.1, 0.5 and -1 for 0° direction are shown in Fig. 3. The S-N diagram in Fig. 3(a) shows that for 0^o specimens at R =

0.1 run out occur at maximum load of 30% of Xt. Also as can be seen from S-N diagram in Fig. 3(b) for 0^o specimen at R = 0.5 the run out is at maximum load of 30% of Xt.

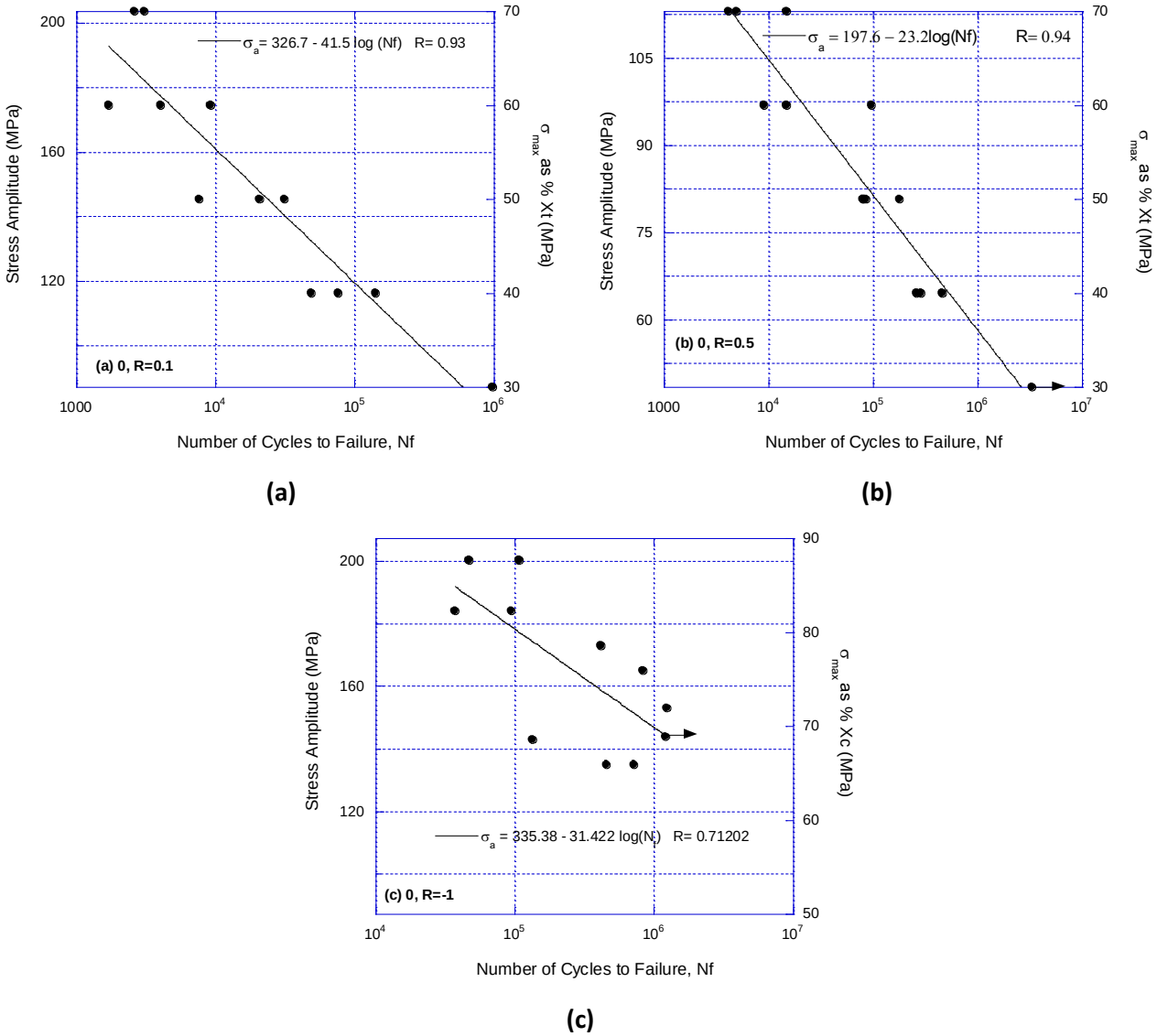

Fig. 3. S-N diagram for T-T loading in 0° direction (a) R=0.1, (b) R=0.5 and (c) R=-1.

The results of the S-N diagram for specimens under T-T loading at R= 0.1 and 0.5 for 90° are shown in Fig. 4. The S-N diagram in Fig. 4(a) shows that the run out for 90^o specimen at R = 0.1 occurs at maximum load of 30% of Yt and from Fig. 4(b) at R = 0.5 the run out happens at maximum load of 30% of Yt.

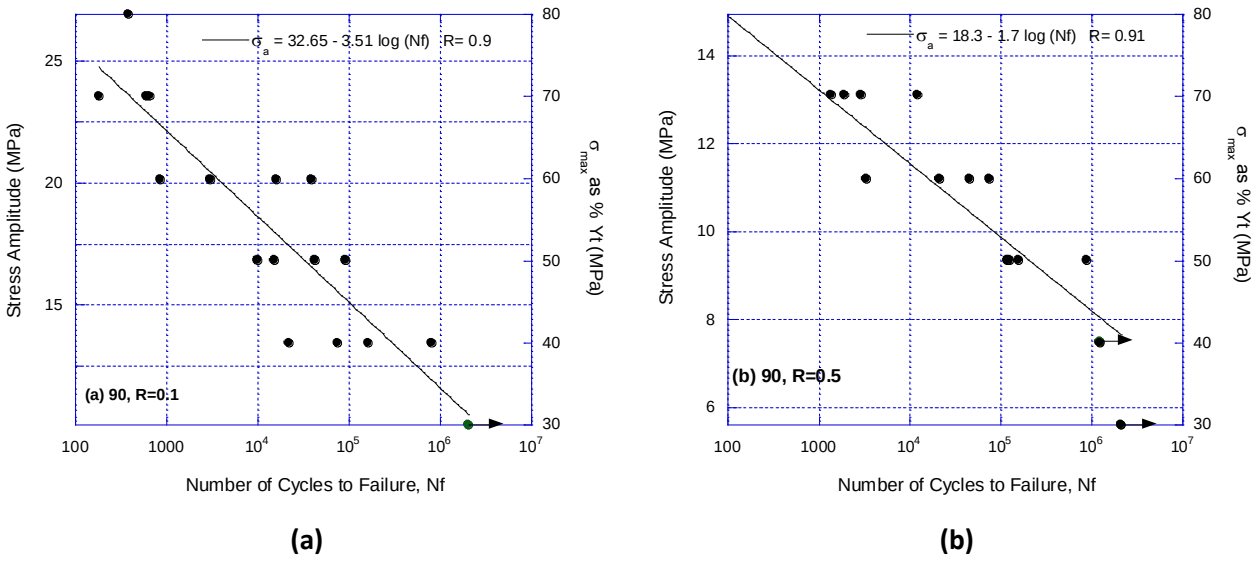

Fig. 4. S-N diagram for T-T loading in 90° direction (a) R=0.1 and (b) R=0.5.

The results of the S-N diagram for specimens under T-C reverse loading at R= -1 for 90° are shown in Fig. 5(a). The results of the S-N diagram for specimens under C-C loading at R= 10 for 90° are shown in Fig. 5(b). The tests were conducted from minimum stress equal to 40% of Yc. The results of the S-N diagram for specimens under C-C loading at R= 2 for 90° are shown in Fig. 5(c).

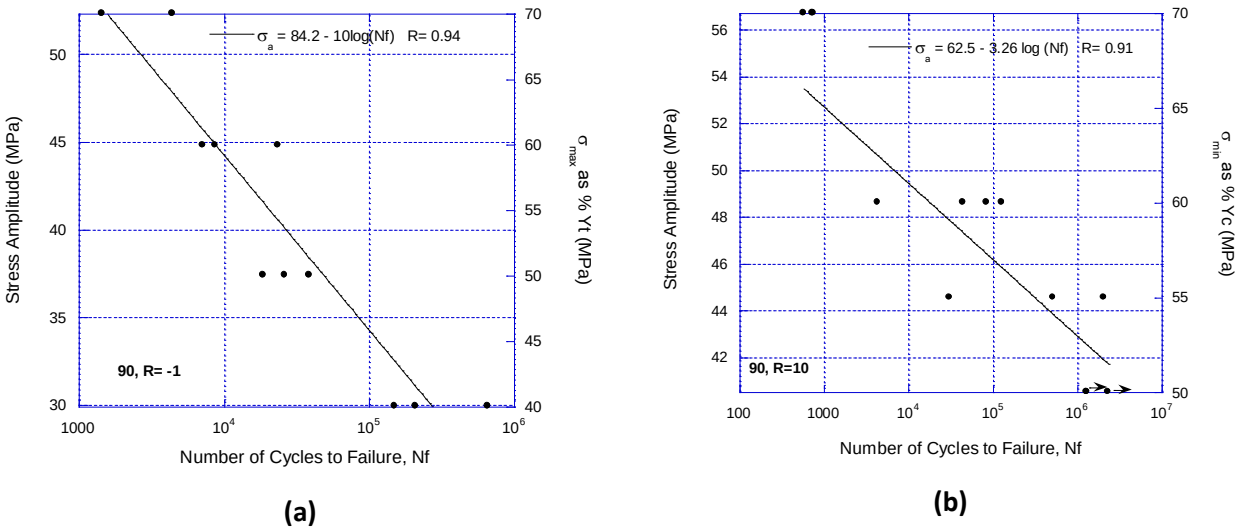

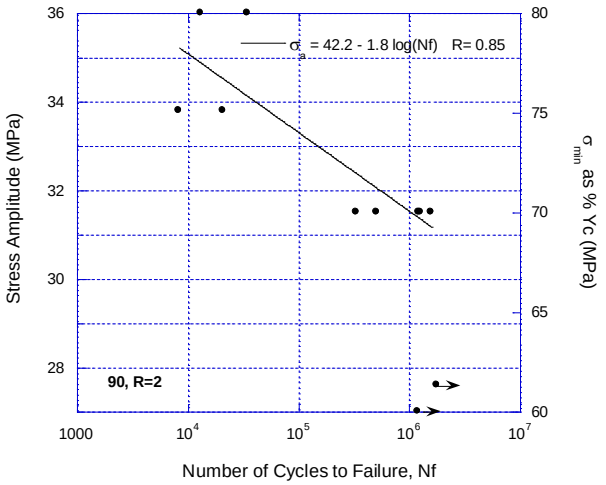

(c)

Fig. 5. S-N diagram for 90° and 5Hz (a) T-C reverse loading at R=-1 and (b) C-C loading at R=10 and (c) C-C loading at R=2.

The constant *C* and *D* for various R ratios and fibre orientations of exponential law fatigue models in Eq. (1) are summarised in Table 2.

Table 2. Constants C and D of exponential law fatigue model in Eq. (1) for various stress ratios and fibre direction for GFRP composite material.

Loading direction	Stress ratio	C	D
0°	0.1	326.7	41.5
	0.5	197.6	23.2
	-1	335.4	31.4
90°	0.1	32.7	3.5
	0.5	18.3	1.7
	-1	84.2	10
	2	42.2	1.8
	10	62.5	3.3

3.2. Effect of R ratio on failure modes

Failure modes of coupons tested in monotonic uniaxial tensile and compressive loading differ from dynamically tested specimens. In 90° specimens under T-T load ratios of R = 0.1 and 0.5, specimens failed in direction normal to the applied load direction along the fibre direction and through the resin matrix. Few samples broke near the end tabs and some in the middle of the coupons. In 90° coupon specimens subjected to reverse loading of T-C at R

= -1, the specimens failed. Representative failed specimens of 90^{o} coupon at R=2 are shown in Fig. 6. In C-C tests delaminations and splaying plies were dominate feature of the fracture surface.

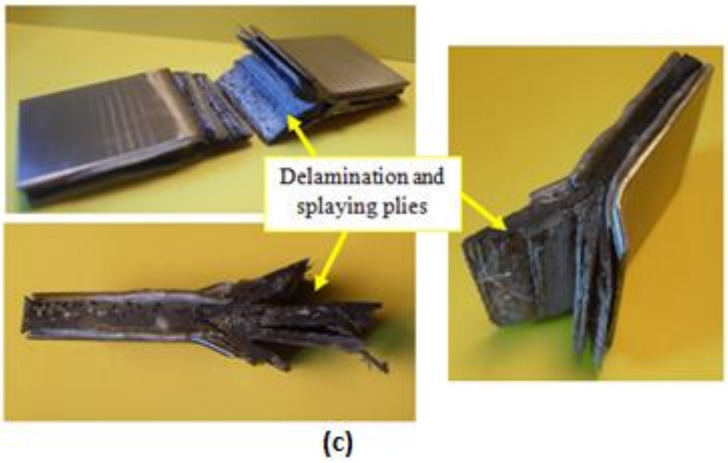

Fig . 6. Failed specimens in fatigue testing for 90° coupons at 5 Hz, R= 2, σ_{max}= 75% of Xc.

In 0° specimens under T-T load at R = 0.1 and 0.5 load ratios, specimens failed by breaking the fibres in an irregular pattern. In these specimens the load transfer between matrix and fibre is reduced by the onset of debonding of fibre/matrix interface, and ultimately fracture occurs by coalescence of interface cracks. For 0^{o} coupon tests subjected to reverse loading under T-C at R = -1, the coupon specimens failed in compression.

4. Stiffness degradation

In FRP composite materials subjected to the cyclic loading, crack density in the transverse direction increases with increasing number of cyclic loading. In the longitudinal direction, due to intraply delamination (matrix splitting along fibres), the damage prevents the load transfer between fibres. As a result fibre failure can occur before reaching to the maximum stress measured in the case of monotonic tensile test which the crack density is lower than in the cyclic loading [17, 2, 1].

Many FRP composite materials follow a stiffness degradation trend similar to the curve schematically shown in Fig. 7.

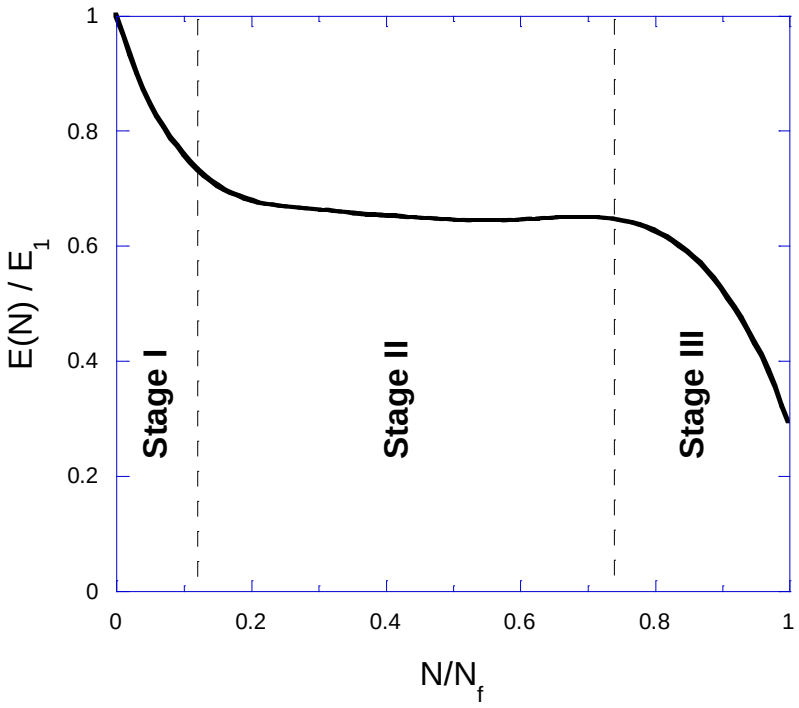

Fig. 7. Stiffness degradation in FRP laminates during fatigue loading.

Schulte [18] identified the three stages shown in Fig. 7 from study on T-T fatigue of cross ply carbon/epoxy laminates. During fatigue loading in stage I a sharp drop in stiffness occurs. In this stage the formation of matrix cracks parallel to the fibres in the transverse direction has been observed very early in the 90° plies which are perpendicular to the loading axis [19]. The development of these transverse cracks dominates the stiffness reduction observed in early fatigue lifetime. Highsmith and Reifsnider [20] reported that in the fatigue tests on FRP composites, the transverse matrix cracks are saturated by reaching to a constant distance between the transverse cracks and this effect is developing after only a few hundred loading cycles.

The damage mechanisms occurring in stage II seem to be unique to fatigue mechanisms, whereas the damage mechanisms which can be observed during stage I, also occur in static tests. A typical mechanism to be observed during stage II is the development of edge delaminations which are the main influencing mechanism for the reduction of the elastic modulus. Besides delamination, additional longitudinal cracks along the fibres in the 0° plies appear which are developed from the transverse cracks in the 90° plies. In stage III a transition to local damage progression occurs. This will cause fibres failure; the result of

which is a sudden drop of stiffness and initiation of final failure. This is the root of the large scatter in fatigue lifetime and why the time of sudden drop in stiffness is hard to predict.

Ferreira, et al. [21] showed that residual stiffness could be an efficient damage metric for the fatigue design models that do not correspond to failure but to a certain percentage of specimen stiffness reduction. Brøndsted et al. [22] studied the fatigue of GFRP composites under block and stochastic loading. They observed the stiffness degradation in stage II could be approximated linearly in terms of stiffness and number of cycles N:

$$\frac{E(N)}{E_1} = AN + B \tag{3}$$

where E(N) is the cyclic modulus after N cycles, E_1 is the initial cyclic modulus, A and B are constants. It was found that the constant A is a function of the stress amplitude, normalized by the static modulus E_0. The rate of change in stiffness then becomes:

$$\frac{d\left(\frac{E(N)}{E_1}\right)}{dN} = -K\left(\frac{\sigma_a}{E_0}\right)^n \tag{4}$$

Therefore stiffness degradation can be expressed by [23, 22]:

$$\frac{E(N)}{E_1} = 1 - K\left(\frac{\sigma_a}{E_0}\right)^n N \tag{5}$$

where K and n are material constants and they are determined by curve fitting of the respective experimental data for $E(N)/E_1$, which depend on the number of stress cycles, N, and the level of applied cyclic stress amplitude, σ_a. By reordering Eq. (5) the material constants K and n can be found in the following form:

$$\frac{1-\frac{E(N)}{E_1}}{N} = K\left(\frac{\sigma_a}{E_0}\right)^n \tag{6}$$

Eq. (6) establishes a stiffness-based design criterion since for a predetermined value of $p = \frac{E(N)}{E_1}$, one can solve for σ_a to obtain design curve corresponding not to material failure but to a specific stiffness degradation percentage $(1-p)\%$.

The experimental results of stiffness degradation at stress ratios of R =0.1, 0.5 and 10 in 0° direction are shown in Fig. 8(a). The stiffness degradation is highest in R=0.1 and lowest in C-C case at R=10. In C-C loading after some initial degradation of stiffness at early cycles, the stiffness remains nearly unchanged throughout loading cycles until the FRP material fails at

the end of its fatigue lifetime. The higher the applied loading or the lower the stress ratio R, will results in faster damage progression. After saturation of the crack density in the matrix, the rate of damage progression becomes steady and slow in stage II. During the final stage III of fatigue life, fibre breakage controls the damage progression. The higher the fracture rate of the fibres will cause a shorter fatigue lifetime. In stage III with an increase in the numbers of fractured fibres, the rate of damage progression of material increases again.

Representative experimental results of stiffness degradation at R=0.1, 0.5, -1, 2 and 10 ratios in 90° direction are shown in Fig. 8(b). The stiffness degradation is the highest in R=0.1, 0.5 and -1 when the maximum applied stress is set at 50% tensile strength Y_t. The lowest stiffness degradation occurs in C-C case at R= 2 and 10 when minimum stress is set at 50% of compressive strength Y_C. Similar to loading in fibre direction, in C-C loading in normal to fibre direction after some initial degradation of stiffness at early cycles, the stiffness remains unchanged throughout loading cycles until the FRP material fails.

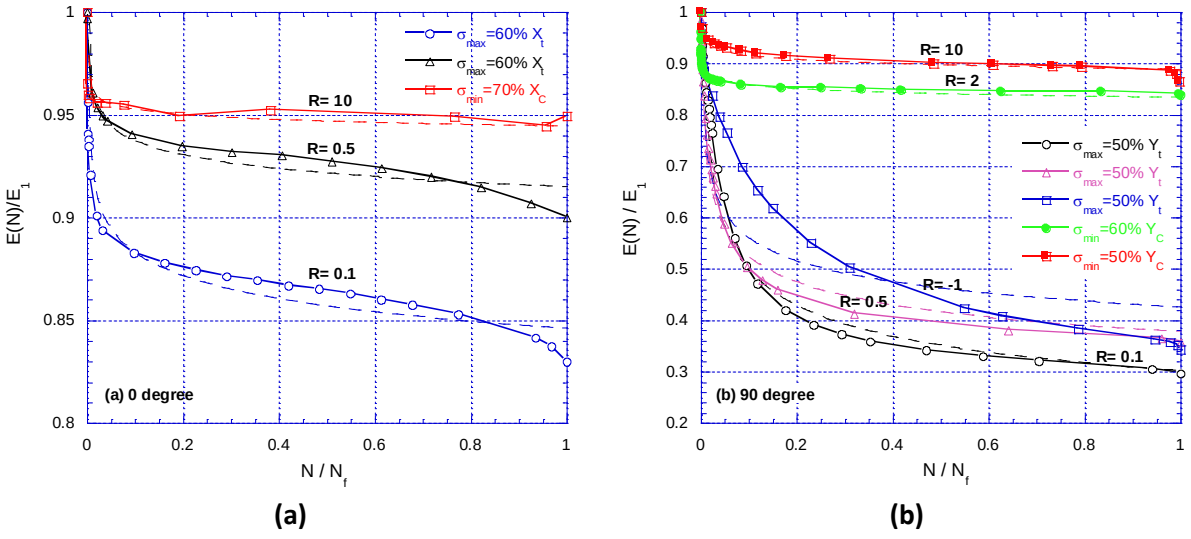

Fig. 8. Stiffness degradation at various R ratios in (a) fibre direction and (b) normal to fibre direction. Solid line experiments, dash line power law trend.

The specific stiffness degradation level, $E(N)/E_1$, for the specimens tested in this work can be calculated from:

$$\frac{E(N)}{E_1} = K\left(\frac{N}{N_f}\right)^{-n} \tag{7}$$

The value of K and n for different specimens and different R ratio are tabulated in Table 3.

Table 3. Constants K and n of power law stiffness degradation model in Eq. (7) for various stress ratios and fibre direction for GFRP composite material.

Loading direction	Stress ratio	K	n	Correlation coefficient
0°	0.1	0.846	0.0186	0.974
	0.5	0.915	0.0105	0.977
	-1	0.945	0.004	0.887
90°	0.1	0.3	0.216	0.967
	0.5	0.38	0.142	0.97
	-1	0.43	0.12	0.82
	2	0.835	0.126	0.962
	10	0.89	0.013	0.96

5. Hysteresis Loop

During cyclic loading FRP material experience hysteresis ellipse shaped loop due to the viscoelastic characteristics of the polymer matrix and friction between debonded and delaminated surfaces. The slope of maximum peak to minimum peak of the load-displacement curve (i.e., dynamic stiffness) decreases from the initial first cycle with a value of K_1 to a value of K(N) during cycle N, which represents stiffness degradation. Shifting of the load-displacement curve (i.e., ratcheting deformation due to cyclic creep of the polymeric matrix) has also been observed to occur in FRP matrix composite materials during stress controlled cyclic loading (see Fig. 9).

As fatigue damage accumulates under fixed amplitude load control, laminates become more compliant, resulting in changes in the amplitude of fatigue strains. Fig. 9 shows hysteresis loop for T-T cyclic loading at R=0.1 for 0° and 90° fibre orientations. In both fibre directions both the maximum and minimum cyclic strains are increased positively.

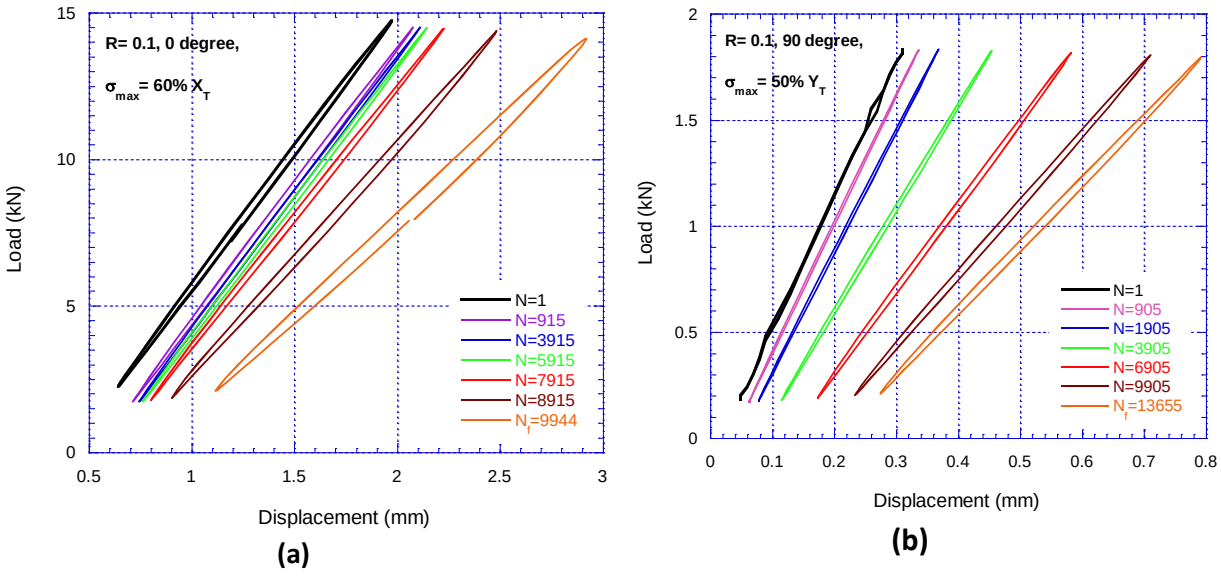

Fig. 9. Hysteresis loop showing ratcheting deformation at R=0.1 (a) for 0° specimens at σ_{max} set at 60% of X_t and (b) for 90° specimens and σ_{max} set at 50% of Y_t.

The T-C reverse loading (R=-1) hysteresis loops for 0° and 90° fibre orientations are shown in Fig. 10. For 0° specimens although the maximum cyclic strain increased positively, but the minimum cyclic strain remained unchanged except at initial cycles while the dynamic stiffness continuously decreases due to positive increase of maximum strain in tension part of the cyclic loading. This suggests that the minimum cyclic strain in compression part does not change and the main contributor to stiffness degradation of the laminate is the tension part of loading cycle. The hysteresis loops for T-C reverse loading for 90° specimen is shown in Fig. 10(b). Although the maximum cyclic strain increased positively, but the minimum cyclic strain remained unchanged. This suggests that in compression part ratcheting deformation does not occur. For 90° specimens at high cycle the load-displacement becomes nonlinear. For both 0° and 90° cases the dynamic stiffness continuously decreased during cyclic loading.

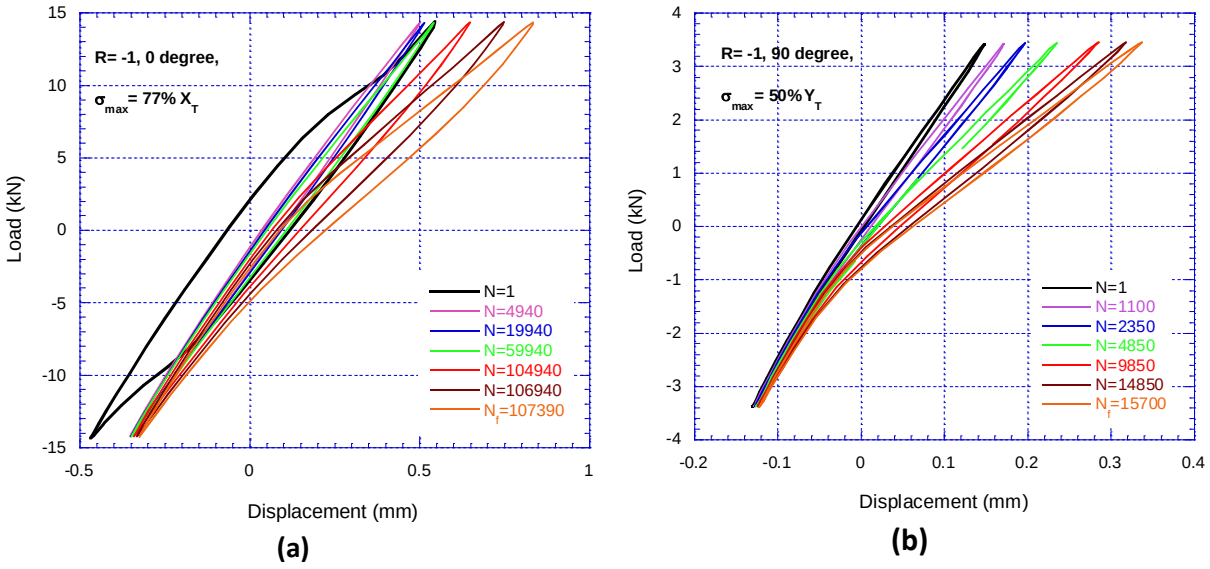

Fig. 10. Hysteresis loop showing ratcheting deformation on tension part of loading at R=-1 (a) for 0° specimens at σ_{max} set at 77% of X_t and (b) for 90° specimens and σ_{max} set at 50% of Y_t.

Fig. 11 shows hysteresis loop for 90° specimens in C-C at R=2 and 10. In both cases the absolute maximum and minimum cyclic strains are increased. However, the increase at R=2 is much higher than R=10. In both compression cases the stiffness of the laminate does not deteriorate and remain linear.

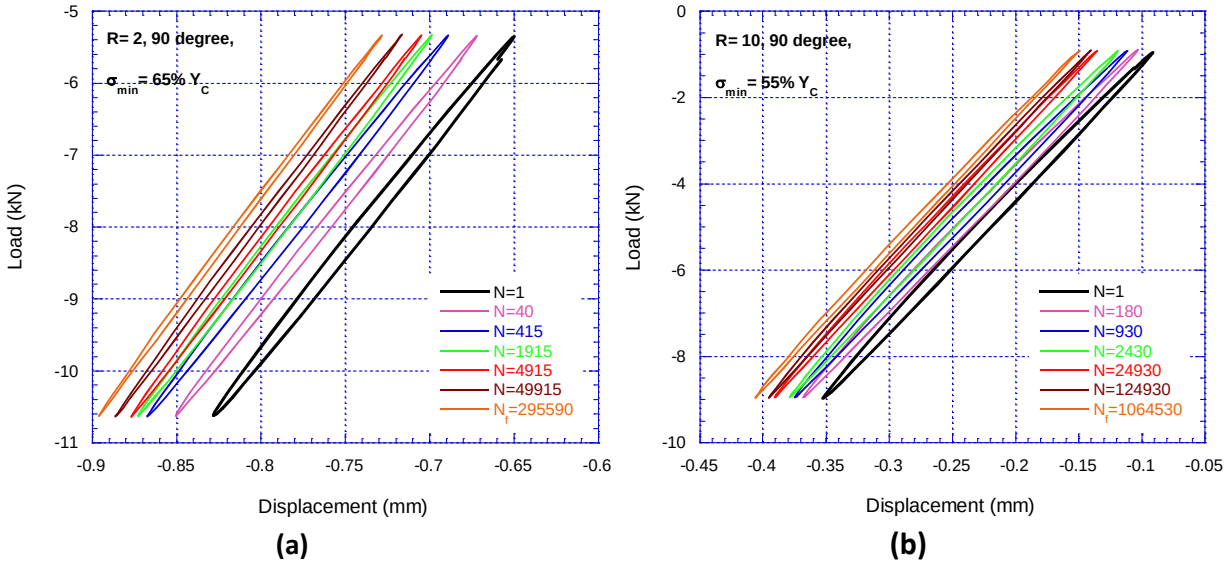

Fig. 11. Hysteresis loop for 90° specimens at (a) R= 2 and σ_{min} set at 65% of Yc and (b) R= 10 and σ_{min} set at 55% of Y_C.

The energy dissipated per cycle is calculated by integrating the area of captured hysteresis loops. The dissipated energy during fatigue lifetime for fatigue loading in fibre and normal to fibre directions at various R ratios and maximum stress are examined in Fig. 12.

Figs. 12 (a) and (b) compare dissipated energy of 0° and 90° fibre directions at R=0.1. For 0° degree loading the energy dissipation remains nearly constant for the majority of the fatigue lifetime and the energy dissipated most at the end of the life, but the increase in energy dissipation in 90° degree direction occurs at a much earlier time and especially at 60% Y_t loading the dissipation energy start from initial cycles. The magnitude of dissipated energy in 0° direction is an order of magnitude higher than in 90° direction.

Figs. 12 (c) and (d) compare dissipated energy of 0° and 90° fibre directions for reverse loading at R=-1. For 0° degree loading at R=-1 the energy dissipation continuously decreases for the majority of the fatigue lifetime but near the end of the fatigue lifetime the energy dissipation increases sharply. In contrast, for 90° degree direction the energy dissipation remains nearly constant until near the end of the fatigue lifetime which it increases sharply, irrespective of the maximum stress.

Figs. 12 (e) and (f) compare dissipated energy of 90° fibre directions at R=2 and 10. For stress ratio of R=2, the dissipated energy continuously decreases during the fatigue lifetime except at σ_{min}=75%Y_C case where near the end of the fatigue lifetime the energy dissipation increases sharply. For stress ratio of R=10, the dissipated energy remains nearly unchanged until around 1000 cycles and after that it decreases for low loads but it is increasing at σ_{min}=70%Y_C.

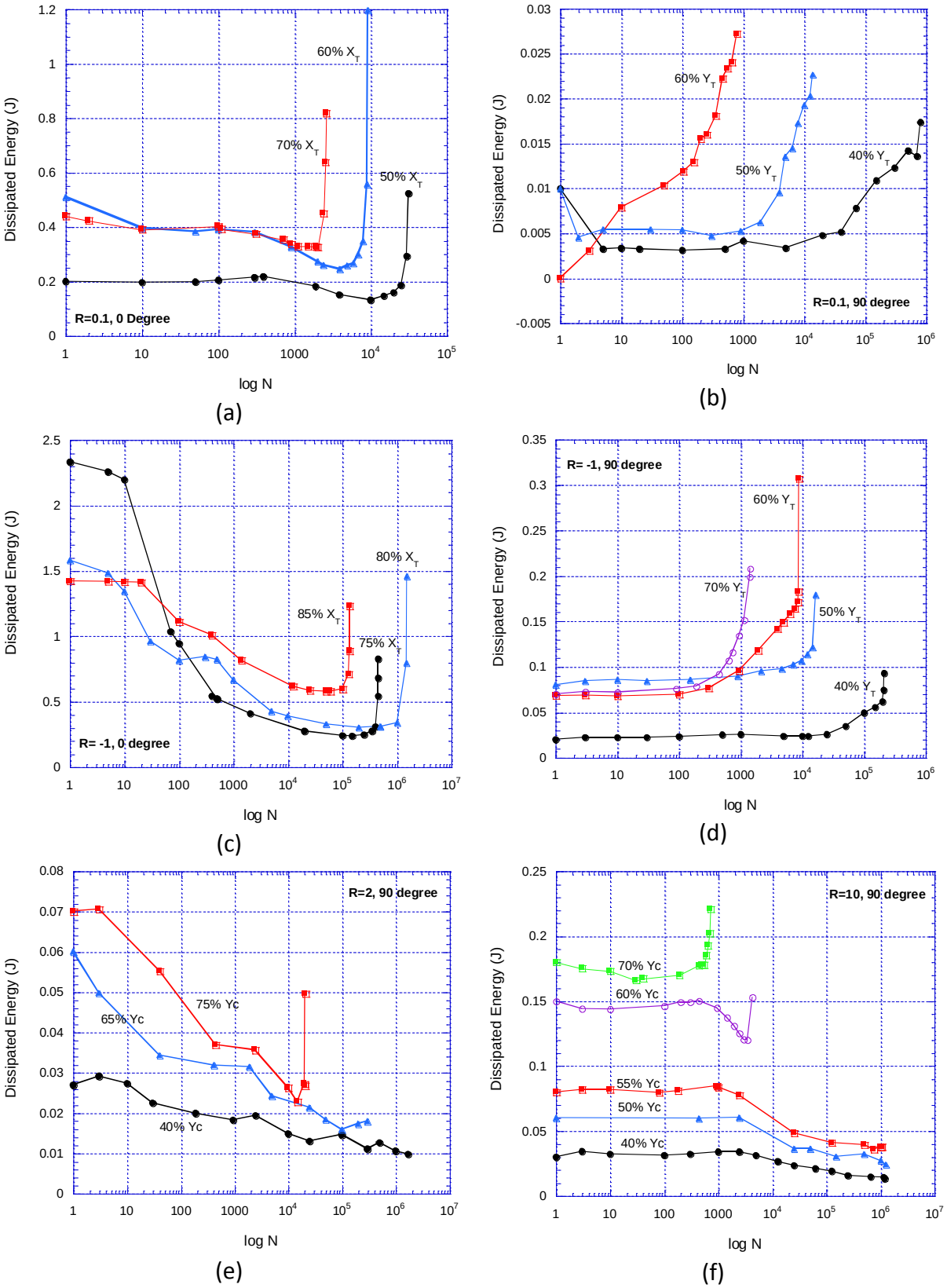

Fig. 12. Dissipated energy during cyclic loading for specimens with σ_{max} set at various percentage of tensile/compressive strength at (a) 0°, R=0.1, (b) 90°, R= 0.1, (c) 0°, R= -1, (d) 90°, R= -1, (e) 90°, R= 2 and, (f) 90°, R= 10.

6. Conclusion

A comprehensive understanding of fatigue performance of FRP laminates is fundamental for proper design of a long lasting structures subjected to variable loading. Many studies on analysis of fatigue of fibre reinforced polymer composite materials have been done in the past to predict damage evolution with various fibre and matrix types under constant amplitude to spectrum loading.

In the present work the fatigue behaviour of laminated GFRP composite material was experimentally examined under load ratios of 0.1, 0.5, -1, 2 and 10 in order to investigate the effect of different load ratios on fatigue lifetime, stiffness degradation and hysteresis loops. The S-N diagrams at various R ratios have been obtained and they showed a nearly linear behaviour in both 0° and 90° directions. The coefficients of exponential fatigue law model used for describing S-N diagram at various R ratios at 0°and 90° fibre directions were determined. In addition the detailed pattern of stiffness degradation and energy dissipation during the loading cycles of these tests are investigated.

The damage evolution under quasistatic and fatigue loading are quite different and this imposes a considerable challenge for understanding the behaviour of FRP laminates. The results of studying the stiffness degradation at various R ratios show that conventional polymeric composites do not typically have a fatigue limit, but instead damage progresses during the entire lifetime of the material and its evolution depends on fibre orientation, R ratio and maximum cyclic stress. However, it has been recently shown that some polymeric composites do exhibit a fatigue threshold or a high cycle fatigue strength (HCFS), which may be due to a damage saturation state at lower applied stresses hindering the onset of failure [24].

In this work from the results of various fatigue tests performed on several specimens; the stiffness degradation of the different specimens has been monitored. The experimental results reveal that in 0° direction specimens under T-T loading (R=0.1 and 0.5) the stiffness decreases gradually with the number of stress cycles in stage II but the speed of degradation is very high at early fatigue lifetime in 90° direction (see Fig. 8). The fatigue lifetime in stage I

for C-C is shorter than stage I in T-T and T-C. In C-C loading, initially stiffness degrades in stage I but in stage II there is almost no variation in stiffness. It is reported that unidirectional fibre composite in general are weaker in compression fatigue [25]. This is not evident from the stiffness point of view.

The experimental cyclic load-displacement data of GFRP material exhibits hysteresis loops. The results of T-T fatigue loading show that in 0° and 90° directions at R=0.1 ratcheting deformation due to cyclic creep of the polymeric matrix occur (see Fig. 9). However, the magnitude of ratcheting deformation in 90° direction is higher than in 0° direction as expected because of polymer matrix deform more easily in 90° direction. Also in both cases the stiffness degradation occurs, but due to crack saturation in transverse direction, the degradation of stiffness in 90° direction is higher. In reverse cyclic loading at R=-1 the stiffness degradation occurs mainly in tension part of the loading cycles and in the high compression part of loading cycle the minimum strain remains unchanged. In C-C fatigue tests at R=2 and 10, except at very early cycles the stiffness remains nearly unchanged and GFRP material does not lose its stiffness. In both C-C fatigue loading ratcheting deformation observed at both R=2 and 10, but the ratcheting is higher at R=2. This is evidence of damage accumulation in the matrix.

The energy dissipated per cycle are calculated by integrating the area of captured hysteresis loops throughout fatigue tests for fatigue loading in fibre and normal to fibre directions at various R ratios and maximum stress. It is shown that for 0° and 90° fibre directions at R=0.1 the energy dissipation remains nearly constant for the majority of the fatigue lifetime and the energy dissipated most near the end of the life, but the increase in energy dissipation in 90° degree direction occurs at a much earlier time. For 0° degree loading at R=-1, the energy dissipation continuously decreases for the majority of the fatigue lifetime but near the end of the fatigue lifetime the energy dissipation increases sharply. In contrast for 90 degree direction the energy dissipation remains nearly constant until near the end of the fatigue lifetime which it increases sharply, irrespective of the maximum stress.

The dissipated energy of 90° fibre directions at C-C loading at R=2 shows that the dissipated energy continuously decreases during the fatigue lifetime except at very high loading of

σ_{min}=75%Y_C case where near the end of the fatigue lifetime the energy dissipation increase sharply. For stress ratio of R=10, the dissipated energy remains nearly unchanged until around 1000 cycles and after that it decreases for low loads but it is increasing at σ_{min}=70%Y_C.

In summary the experimental results demonstrated that the dissipated energy during the fatigue lifetime is dependent on R-ratio, maximum cyclic stress and fibre orientation. However, in majority of the cases, the energy dissipated per cycle near the end of the fatigue lifetime increases as a result of an increase in the area captured by hysteresis loops.

Acknowledgement

The authors would like to thank technicians at School of Mechanical & Automotive Engineering in Kingston University: Alex Vine and Dean Wells for helping in various mechanical testing.

References

[1] S. L. Ogin, P. A. Smith and P. W. R. Beaumont, “Matrix cracking and stiffness reduction during the fatigue of a (0/90)s GFRP laminate,” *Compos Sci Technol ,* vol. 22, no. 1, pp. 23-31, 1985.

[2] J. Tong, “Characteristics of fatigue crack growth in GFRP laminates,” *Int J Fatigue,* vol. 24, p. 291–297, 2002.

[3] O. Al-Khudairi, H. Hadavinia, A. Waggott, E. Lewis and C. Little, “Characterising mode I/mode II fatigue delamination growth in unidirectional fibre reinforced polymer laminates,” *Materials & Design,* vol. 66, no. A, pp. 93-102, 2015.

[4] K. Gordnian, H. Hadavinia, P. Mason and E. Madenci, “Determination of fracture energy and tensile cohesive strength in Mode I delamination of angle-ply laminated composites,” *Composite Structures,* vol. 82, no. 4, pp. 577-586, 2008.

[5] N. Domun, H. Hadavinia, T. Zhang, T. Sainsbury, G. Liaghat and S. Vahid, “Improving fracture toughness and strength of epoxy using nanomaterials – A review of current status,” *Nanoscale,* vol. 7, no. 23, p. 10294–10329, 2015.

[6] C. M. Manjunatha, A. C. Taylor, A. J. Kinloch and S. Sprenger, “The tensile fatigue behavior of a GFRP composite with rubber particle modified epoxy matrix,” *Journal of Reinforced Plastics and Composites,* vol. 29, no. 14, pp. 2170-2183, 2010.

[7] J. A. Mohandesi and B. Majidi, “Fatigue damage accumulation in carbon/epoxy laminated composites,” *Materials & Design,* vol. 30, p. 1950–1956, 2009.

[8] J. N. Yang and D. L. Jones, “ Effect of load sequence on the statistical fatigue of composite,” *AIAA J,* vol. 18, no. 12, p. 1525–31, 1980.

[9] H. Whitworth, “A stiffness degradation model for composite lamainates under fatigue loading,” *Composite Structures,* vol. 40, no. 2, pp. 95-101, 1998.

[10] M. H. Abd Allah, E. M. Abdin and A. I. Selmy, “Effect of mean stress on fatigue behavior of GFRP pultruded rod composites,” *Composites Part A,* vol. 28A, p. 87–91, 1997.

[11] M. Kawai and K. Kato, “Effects of R-ratio on the off-axis fatigue behavior of unidirectional hybrid GFRP/A1 laminates at room temperature,” *Int J Fatigue,* vol. 28, p. 1226–38, 2006.

[12] Y.-H. Huh, J.-H. Lee, D.-J. Kim and Y.-S. Lee, “Effect of stress ratio on fatigue life of GFRP composites for WT blade,” *Journal of Mechanical Science and Technology,* vol. 26, no. 7, pp. 2117-2120, 2012.

[13] R. D. B. Sevenois and V. Van Paepegem, “Fatigue damage modeling techniques for textile composites: Review and comparison with unidirectional composite modeling techniques,” *Applied Mechanics Reviews,* vol. 67, no. 2, March 2015.

[14] J. A. Epaarachchi and P. D. Clausen, “An empirical model for fatigue behavior prediction of glass fibre-reinforced plastic composites for various stress ratios and test frequencies,” *Composites Part A,* vol. 34, no. 4, pp. 313-326, 2003.

[15] ASTM E739-91, “Standard practice for statistical analysis of linear or linearized stress-life (SN) and strain-life (eN) fatigue data,” 2004.

[16] B. Harris, “A historical review of the fatigue behaviour of fibre reinforced plastics,” in *Fatigue in Composites*, CRC Press, 2003, pp. 3-35.

[17] A. Gagel, D. Lange and K. Schulte, “On the relation between crack densities, stiffness degradation, and surface temperature distribution of tensile fatigue loaded glass-fiber non-crimp-fabric reinforced epoxy,” *Composites Part A,* vol. 37, no. 2, pp. 222-228, 2006.

[18] K. Schulte, E. Reese and T.-W. Chou, “Fatigue behaviour and damage development in woven fabric and hybrid fabric composites,” in *Sixth International Conference on Composite Materials (ICCMVI)*, London, 1987.

[19] W. Van Paepegem and J. Degrieck, “A new approach of residual stiffness and strength for fatigue of fibre-reinforced composites,” *Int J Fatigue,* vol. 24, no. 7, pp. 747-762, 2002.

[20] A. L. Highsmith and K. L. Reifsnider, “Stiffness-reduction mechanisms in composite laminates,” in *Reifsnider, K.L. (ed.). Damage in composite materials ASTM STP 775*, American Society for Testing and Materials, 1982, pp. 103-117.

[21] J. Ferreira, P. Reis, J. Costa and M. Richardson, “Fatigue behaviour of composite adhesive lap joints,” *Compo Sci Techno,* vol. 62, no. 10-11, pp. 1373-1379, 2002.

[22] P. Brøndsted, S. I. Andersen and H. Lilholt, “Fatigue damage accumulation and lifetime prediction of GFRP materials under block loading and stochastic loading,” in *Polymeric composites—expanding the limits. Proceedings of the 18th Risø International Symposium on Materials Science,Risø International Laboratory*, Roskilde, Denmark, 1997.

[23] A. P. Vassilopoulos and T. Keller, Fatigue of Fiber-reinforced Composites, Engineering Materials and Processes, London: Springer-Verlag London Limited , 2011.

[24] C. Colombo, F. Libonati, F. Pezzani, A. Salerno and L. Vergani, “Fatigue Behaviour of a GFRP Laminate by Thermographic Measurements,” *Eng Procedia,* vol. 10, pp. 3518-3527, 2011.

[25] A. N. Towo and M. P. Ansell, “Fatigue of sisal fibre reinforced composites: Constant-life diagrams and hysteresis loop capture,” *Compo Sci Tech,* vol. 68, pp. 915-924, 2007.